Preprints (www.preprints.org) | NOT PEER-REVIEWED | Posted: 3 November 2022 doi:10.20944/preprints202211.0067.v1

*Article*

# Adsorption and Displacement of Methane in Carbon Nanoslits: Insights from Molecular Simulations

**Dias Bekeshov[1], Sultan Ashimov[1], Yanwei Wang[1,2,*], and Lei Wang[3,4,*]**

[1] Department of Chemical & Materials Engineering, School of Engineering and Digital Sciences, Nazarbayev University, Nur-Sultan 010000, Kazakhstan
[2] Laboratory of Computational Materials Science, Center for Energy and Advanced Materials Science, National Laboratory Astana, Nur-Sultan 010000, Kazakhstan
[3] College of Energy, Chengdu University of Technology, Chengdu 610059, China
[4] Department of Petroleum Engineering, School of Mining and Geosciences, Nazarbayev University, Nur-Sultan 010000, Kazakhstan
* Correspondence: yanwei.wang@nu.edu.kz (Y.W.); wanglei@cdut.edu.cn (L.W.)

**Abstract:** Shale gas and coalbed methane are energy sources that partly or even mainly consist of methane stored in an adsorbed state in the pores of the organic-rich rock and coal seams. In this study, the graphene nanoslit model is employed to model the nanometer slit pores in shale and coal. The Grand Canonical Monte Carlo (GCMC) and Molecular Dynamics (MD) modelling methods are used to investigate the mechanisms of adsorption and displacement of methane in the slit pore. It was found that the CVFF forcefield resulted in the largest adsorption amount, while the PCFF forcefield resulted in the least. The COMPASS and COMPASS II force fields led to similar results. As the width of the slit pore increases, the adsorption amount of gas molecules increases, and the number density profile of adsorbed methane molecules alters from a single adsorption layer to multi-adsorption layers. The minimum slit pore width at which methane molecules can penetrate the slit pore was found to be 0.7 nm. Moreover, it is demonstrated that by lowering the temperature, the adsorption rate of the methane increases since the adsorption is an exothermic process. Enhancing methane recovery was investigated by the injection of gases such as $CO_2$ and $N_2$ to displace the adsorbed methane. The comparison of adsorption isotherms of gas molecules provided the following order in terms of the amount of adsorption: $CO_2 > CH_4 > N_2$.

**Keywords:** Methane; adsorption; shale gas; coalbed methane; slit pore; carbon dioxide; modelling; Grand Canonical Monte Carlo; Molecular Dynamics.

## 1. Introduction

Natural gas is a fossil energy resource formed deep beneath the earth's surface through millions of years of geochemical evolution. Natural gas could contain quite a few different gas compounds, in which methane ($CH_4$) is usually the dominant component [1]. Compared to other fossil fuels, such as coal and crude oil, natural gas is a relatively clean energy resource. Based on the technological and economical difficulty involved in exploitation processes, natural gas resources can be classified into conventional and unconventional types, the latter of which nowadays attract more and more attention provided the increasing worldwide energy demand. Two major members of unconventional gas resources are shale gas and coal bed methane (CBM).

Shale gas is an abundant unconventional gas resource that has been booming for almost two decades, thanks to the efficient implementation of horizontal drilling and multistage hydraulic fracturing [2–5]. Large amounts of methane stored in the shale matrix are existing in an adsorption state, especially in the organic nanopores [6,7]. Methane adsorption not only affects the prediction of gas reserve estimation but also depresses the efficiency of production. To improve shale gas and CBM recovery efficiency, gas injection

© 2022 by the author(s). Distributed under a Creative Commons CC BY license.

Preprints (www.preprints.org) | NOT PEER-REVIEWED | Posted: 3 November 2022 doi:10.20944/preprints202211.0067.v1



to displace adsorbed methane and storage in both shale and coal formations has been investigated as a technical option with promising capacity [5,8–10]. Carbon dioxide ($CO_2$) alongside by nitrogen ($N_2$) could be used to displace $CH_4$ from the shale, the process known as *enhanced shale gas recovery (ESGR)* [11–13]. This allows to sequestrate $CO_2$ and to reduce anthropogenic greenhouse gas (GHG) emissions (mostly $CO_2$), and achieve net-zero $CO_2$ emissions by 2050 [14]. Therefore, it is important to study the competitive adsorption mechanisms of methane and injected gas as well as the displacement process in organic nanopores for the evaluation of recoverable gas reserves and efficient production of shale and CBM gas.

The adsorption behaviour of methane has been studied by many researchers. For instance, Wu *et al.* [15] used molecular dynamics (MD) simulations to investigate the adsorption and displacement of methane, carbon dioxide and nitrogen in slit pores composed of graphite slabs and with pore sizes of 7 Å, 10 Å, 15 Å and 20 Å based on the "united atom" models. Lin *et al.* [16] used both MD and Grand Canonical Monte Carlo (GCMC) simulations to study the adsorption of methane at 300 K, 320 K, 340 K and 360 K, and the pressure range of 1 to 40 MPa, with pore sizes of 2 to 11 nm. They also found out that the methane adsorption energy on monolayer graphene is similar to the adsorption energy of shale. Therefore, graphene can be used to represent shale in molecular simulations. Zhao *et al.*[17] performed GCMC simulations at pressures up to 40 MPa and fixed temperature of 333.15 K to investigate the adsorption behaviour of methane in graphite with pore sizes of 1.2 nm, 2.5 nm and 5.5 nm. Taheri and Nakhaei Pour [18] and Xu *et al.*[19] studied the adsorption and diffusion behaviours of methane on different graphene based surfaces by both MD and GCMC methods. Whereas, Cengiz *et al.*[20] examined the adsorption of methane in fullerene pillared graphene nanocomposites using only GCMC method. In a recent study by Cheng *et al.*[21], the displacement of methane by carbon dioxide in nanoslits were explored using the MD method.

Molecular simulations by the MD and GCMC methods [22] are useful tools to investigate shale gas adsorption and to understand the adsorption mechanisms at the detailed microscopic level. It is more cost-effective than conducting experiments physically. Moreover, factors such as temperature, pressure and different molecules can be investigated. Newton's equations of motion are used in the MD method to show the evolution of particles over time. In MD simulations, the positions (coordinates and orientations) and velocities (linear and angular) of the particles are calculated for every step. In the GCMC method, particles are moved randomly and the real trajectories of the system cannot be generated, meaning the system does not develop along a physical path. In both methods, the interactions between atoms are calculated using the forcefield, which collects all the atomic parameters and functions necessary for this calculation. In MD the forces of each atom are computed in parallel, while in GCMC only one particle is moved at a time. The advantage of the GCMC method, on the other hand, is that it directly gives the number of molecules adsorbed in the pore and shows the variation of adsorption amount by pressure. Since the MD method is good for modelling molecular motions and obtaining dynamic information about the system, and the GCMC method is good for calculating the thermodynamic parameters of the system, these two methods can be applied together to get a broader understanding of the system.

## 2. Simulation Model and Methods

### *2.1. GCMC simulations*

#### 2.1.1. Model and simulation details

In constructing the model, the built-in graphene structure in Materials Studio 7.0 was used. The original cell lattice constant is as follows, a=2.46 Å, b=4.26 Å, c=30 Å, $\alpha = \beta = \gamma$ = 90°. The nanoslit was created using the 24a × 5b supercell, which created the size in the $x \times y$ directions of 59.03 Å×21.3 Å. The slit pore size in the z direction was determined by different $H$ values (0.85 nm, 1.00 nm, 1.50 nm and 2.00 nm). To ensure the periodicity of the

Preprints (www.preprints.org) | NOT PEER-REVIEWED | Posted: 3 November 2022 doi:10.20944/preprints202211.0067.v1



structure the model was constructed in the form of a periodic rectangle with a pore size H and a space above and below it with a height of $H/2$ as shown in Fig. 1.

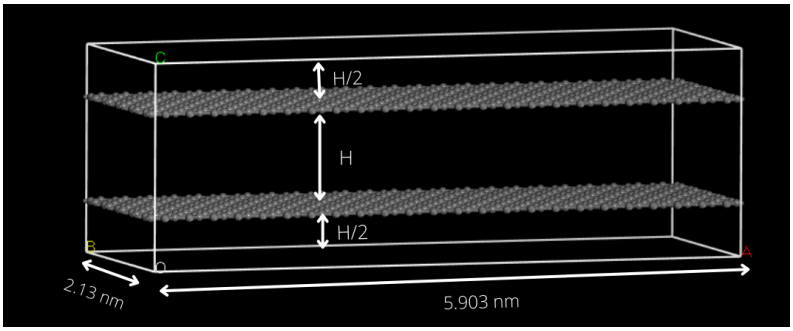


**Figure 1.** Representative model of the nanoslit with the pore size 1 nm used in GCMC simulations.

The simulation of the adsorption isotherm was conducted using the GCMC method. The Metropolis sampling method was used to obtain a sequence of random samples and production steps of 100000 and equilibration steps of 10000 were used to ensure good quality. The forcefield which was used for the simulations is Condensed-phase Optimized Molecular Potentials for Atomistic Simulation Studies II (COMPASS II) with forcefield assigned charges. The Ewald method was used to calculate the electrostatic force, and the atom-based method was used to calculate the Van der Waals force with the cutoff distance of 12.5 Å. To make the model similar to the shale reservoir, the temperature was set as 318 K and the pressure range of 0 to 40 MPa was used. The GCMC simulations on all pore sizes were conducted with $CH_4$, $CO_2$, and nitrogen ($N_2$) molecules. The unit of the adsorption amounts obtained from simulations is molecules per unit cell. In order to compare the adsorption of molecules with other similar studies and experiments, it is converted to millimoles per gram ($mmol \cdot g^{-1}$).

To find out the dependence of adsorption amount on forcefields, the GCMC simulations for methane of pore size 10 Å and temperature 298 K were conducted for the COMPASS, COMPASS II, CVFF and PCFF forcefields. Finally, the effect of different temperatures on adsorption amounts was analyzed. The GCMC simulations of methane molecule for the pore size of 1 nm were conducted with the temperatures of 273 K, 283 K, 293 K, 303 K, 313 K and 333 K using the COMPASS II forcefield.

### 2.1.2. Data analysis: Adsorption isotherms

Adsorption isotherm is one of the most important aspects of understanding the adsorption process. It is useful in optimizing the adsorption process, describing the properties of adsorbents and in designing the adsorption systems [23]. Adsorption isotherm is described as the total amount of gas molecules present in the pore space as a function of pressure at a constant temperature. It includes both the gas molecules adsorbed on the surface of the graphene walls as well as the molecules in the centre of the pore [24].

An adsorption model is essential for describing the adsorption process and determining the maximum adsorption amount. For this reason, numerous adsorption models, that are based on various theories, including monolayer adsorption, multilayer adsorption and micropore filling, have been developed over the years [25]. The data obtained from molecular simulations were fitted with two commonly used isotherm models, Langmuir and Freundlich. In order to find the adsorption model that best describes the adsorption of gas molecules on a graphene surface, the coefficient of regression, $R^2$, is used.

In this work, adsorption isotherms were analyzed using the Langmuir model and the Freundlich model, both commonly used in the analysis of gas adsorption [23,26]. The Langmuir equation is given as [26]:

$$q_e = \frac{q_s K_L P}{1 + K_L P} \tag{1}$$

Preprints (www.preprints.org) | NOT PEER-REVIEWED | Posted: 3 November 2022 doi:10.20944/preprints202211.0067.v1



where $q_e$ is the adsorption amount in mmol $\cdot$ g$^{-1}$, $q_s$ is the maximum adsorption amount in mmol $\cdot$ g$^{-1}$, $K_L$ is the Langmuir adsorption constant in MPa$^{-1}$, $P$ is the equilibrium pressure in MPa. The Freundlich equation is given as [26]:

$$q_e = k_F P^{1/n} \tag{2}$$

where $k_F$ is the Freundlich isotherm constant in mmol $\cdot$ g$^{-1}$ $\cdot$ MPa$^{-1/n}$ and $n$ is the heterogeneity factor that represents a deviation from the linearity of adsorption, and is also known as the Freundlich coefficient [26].

#### 2.1.3. Data analysis: Excess adsorption & isosteric heat

Excess adsorption is described as the extra amount of gas molecules that are absorbed in comparison to the amount of gas that would be present in the same pore volume in the absence of pore walls [24]. According to Mosher *et al.* [24] the extra gas density in the system as a result of adsorption is calculated by deducting the expected gas density in the volume from the total adsorption since the gas in the adsorbed phase has a higher density than the same gas in the bulk phase. Thus, the excess adsorption amount ($n_{ex}$ in unit of mmol $\cdot$ g$^{-1}$) can be calculated using this formula [27]:

$$n_{ex} = N - \rho_g V_p M^{-1} \tag{3}$$

where $N$ is the total amount of gas in mmol $\cdot$ g$^{-1}$, $\rho_g$ is the equilibrium density of the gas in g $\cdot$ cm$^{-3}$, $V_p$ is the free volume in the pore in cm$^3$ $\cdot$ g$^{-1}$, and $M$ is the molar mass in unit of g $\cdot$ mmol$^{-1}$. The free volume is determined using the method proposed by Talu and Myers [28]. They used helium as a reference gas, assuming it is not adsorbed to the walls [29]. The equilibrium densities for all the gases were calculated using the Soave-Redlich-Kwong (SRK) equation of state [30].

Another important quantity used to study the adsorption process is the heat of adsorption, which is the energy released when molecules transfer from bulk to adsorbed state [31]. It represents the strength of attraction of the adsorbate into the solid adsorbent surface [32]. Depending on the strength of the interaction between the adsorbate and adsorbent, the adsorption process is subdivided into chemisorption and physisorption [33]. All weak electrostatic interactions, such as dipole-dipole and London forces, as well as Van Der Waals interactions, are collectively referred to as physisorption [33]. Chemisorption, on the other hand, occurs when the covalent bond between the adsorbate and adsorbent is formed as a result of electron sharing or transferring [33]. Chemisorption mainly involves monolayer surface coverage, while physisorption can entail either monolayer or multilayer surface coverage [29].

The isosteric heat of adsorption $Q_{st}$ (kcal/mol) at a given loading is obtained from the Clapeyron equation:

$$Q_{st} = RT \frac{d(\ln p)}{d(\ln T)} \tag{4}$$

where $p$ is the pressure value in kPa, $T$ is the temperature value in K, $R$ is the universal gas constant (8.314 J/K·mol). Similarly, other studies used the Clausius-Clapeyron equation to calculate the isosteric heat from adsorption isotherms [34,35]. For simplicity in comparing the isosteric heats with other studies, it is converted to kJ/mol and plotted against loading in mmol $\cdot$ g$^{-1}$.

### *2.2. MD Simulations*

Complex structures of nanoslits in shales were modelled, as slit pores, consisting of two disconnected and fixed graphite plates saturated with hydrogen atoms at the edges (see Fig. 2). 6 Å, 7 Å, 10 Å, 15 Åand 20 Å of the inter-layer distances ($H$) were selected to investigate the effect of slit pores width on the methane adsorption. In constructing the model, the built-in graphene structure in Materials Studio 7.0 was used. It was given as a supercell with triclinic lattice type and dimensions of $a$ = 2.46 Å, $b$ = 4.26 Å, $c$ = 30 Å, $\alpha$ =

Preprints (www.preprints.org) | NOT PEER-REVIEWED | Posted: 3 November 2022 doi:10.20944/preprints202211.0067.v1



$\beta = \gamma = 90°$. Methane ($CH_4$), $CO_2$ and $N_2$ gas molecules were constructed by sketching atoms. All three molecules and also the graphene layer were optimised geometrically using the COMPASS II force field.

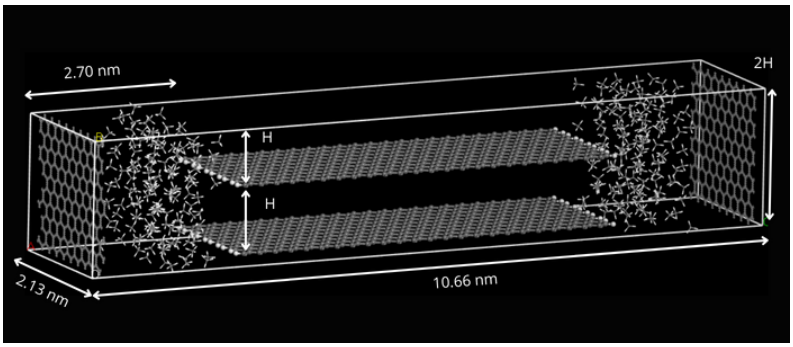


**Figure 2.** Schematic illustration of a representative adsorption model used in MD simulations, where *H* indicated inter-layer distances. Periodic boundary conditions are used.

The bulk phase of methane was prepared with a vertical graphene layer on one side and connected to a slit pore on the other side to simulate methane adsorption. The amorphous cell was constructed in a such way that the lengths of a and b were equal to the width and height of the box, respectively 2.13 nm for the a value and depending on the slit pore size the b value was selected as 1.2 nm, 1.4 nm, 2 nm, 3 nm and 4 nm. The amount of methane in the bulk phase was based on the density of the amorphous cell which was equal to 0.657 $g/cm^3$ to obtain approximately the same pressure. Schematic illustration of a representative adsorption model used in MD simulations is given in Fig. 2. Under the pressure of the bulk phase of methane, due to the attraction potentials, methane molecules enter the slit pore and start to adsorb on the walls. The simulations were conducted in the canonical ensemble with a total simulation time of 2 ns. The temperature is controlled by a Nosé-Hoover thermostat. At the same time, the influence of temperature in the range of 0 to 80 $^0$C was investigated.

To simulate the displacement process of adsorbed methane by gas injections, the slit pore after the adsorption process is connected with the bulk phase of injection gases. Due to the pressure difference, the injected gases enter the slit pore and displace adsorbed methane. Simulations were conducted in the NVT ensemble with a total simulation time of 2 ns and sampling frequency of 0.02 ns. The temperature is controlled by a Nosé-Hoover thermostat. The influence of temperature on the density profile was investigated. Radial distribution functions (RDFs) and methane densities profiles were calculated to explore the structural information (see Fig. 3) for the adsorbed $CH_4$, $CO_2$ and $N_2$ in the graphene slit pore.

Simulations for a pore size of 1.5 nm at 293 K were selected as a case study to analyze the RDFs. The trajectory for the RDF analysis was selected in a such way that the data were analyzed only after equilibration - the last 200 ps (20 frames). Sets between carbon (graphene) - $CH_4$, $CO_2$ and $N_2$ were studied with cutoff distance of 2 nm and interval of 0.02 nm. Periodic self-interactions were included. Note that for those analyses all three molecules were introduced as particles, while carbon was selected as a distinct atom of the graphene layer.

The influence of temperature and slit pore size on methane adsorption and its displacement by $CO_2$ and $N_2$ gases were analyzed based the simulation snapshots of the last 200 ps (20 frames). The trajectory was selected in a such way that the data were analyzed only after the profile reaches a steady result. After obtaining raw profiles, the direction of (0 1 0) was selected to get the relative concentration of the methane on the Y-axis (vertical axis). The relative concentration was converted to number density by dividing each value by the volume of the cell.

Preprints (www.preprints.org) | NOT PEER-REVIEWED | Posted: 3 November 2022 doi:10.20944/preprints202211.0067.v1



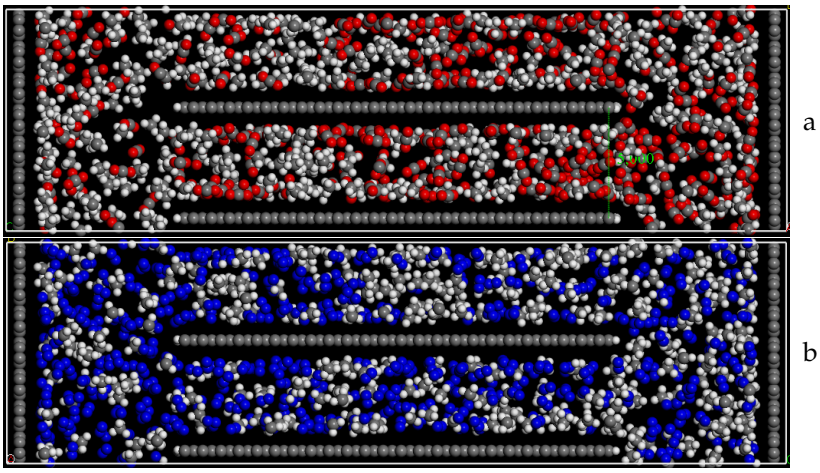


**Figure 3.** Simulation snapshots by the end of the displacement of $CH_4$ by a) $CO_2$ and $N_2$ at temperature of 293K and pore size of 1.5 nm.

## 3. Results & Discussion

### *3.1. Influence of forcefield on methane adsorption*

Before doing the main simulations, the influence of different forcefields on methane adsorption has been studied and demonstrated in Fig. 4. The following results were obtained from these simulations: CVFF gives the largest adsorption amount, while PCFF shows the least. COMPASS and COMPASS II, on the other hand, demonstrate similar results, showing a slight deviation. COMPASS and COMPASS II are more recent forcefields. According to Khalkhali *et al.* [36], the results obtained using the COMPASS and COMPASS II forcefields are in better agreement with the experimental data. That is why COMPASS II forcefield has been used in this study to predict the adsorption of methane.

Concerning the adsorption isotherm model, it can be observed from Tables 1 and 2 that the coefficient of regression, $R^2$, is higher for Langmuir model, meaning it is more accurate at predicting the adsorption amount. Thus, in this paper, the Langmuir isotherm model is used in fitting the simulation results. Moreover, Rexer *et al.* [37], Zhao *et al.* [17], Zhou *et al.* [38] and many other researchers have also used the Langmuir isotherm model to analyze their adsorption data.

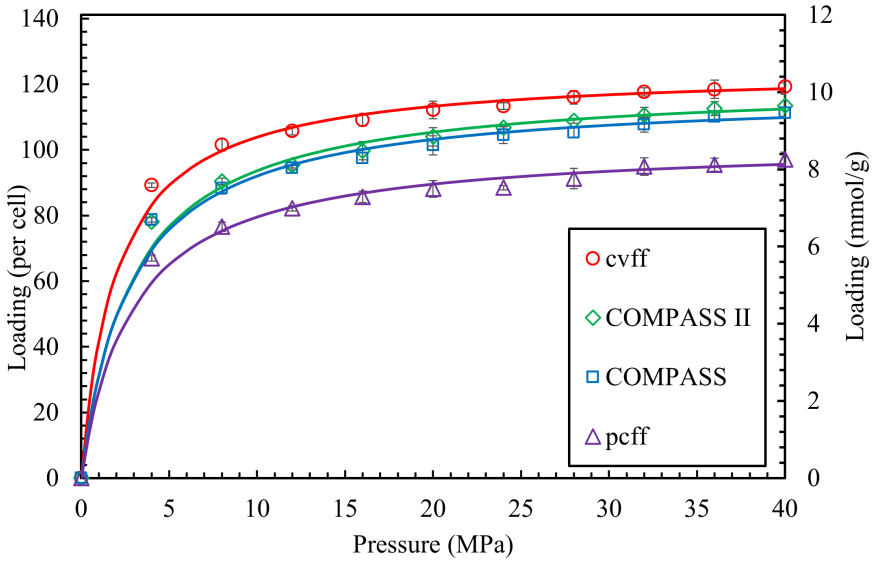


**Figure 4.** Adsorption isotherms of $CH_4$ molecule for the pore size of 1 nm, temperature of 298 K and different forcefields. Symbols are simulation results, and solid lines are Langmuir fittings.

Preprints (www.preprints.org) | NOT PEER-REVIEWED | Posted: 3 November 2022 doi:10.20944/preprints202211.0067.v1



**Table 1.** Fitting parameters of the Langmuir model (see Eq. (1)) for the pore size of 1 nm, temperature of 298 K and different forcefields, where $q_s$ is the maximum adsorption amount in mmol $\cdot$ g$^{-1}$, $K_L$ is the Langmuir adsorption constant in MPa$^{-1}$.

| | CVFF | COMPASS | COMPASS II | PCFF |
|---|---|---|---|---|
| $q_s$ | 10.5865 | 9.9807 | 10.2515 | 8.7132 |
| $K_L$ | 0.5032 | 0.3628 | 0.3489 | 0.3467 |
| $R^2$ | 0.9996 | 0.9986 | 0.9991 | 0.9981 |

**Table 2.** Fitting parameters of Freundlich model (see Eq. (2)) for the pore size of 1 nm, temperature of 298 K and different forcefields, where $k_F$ is the Freundlich isotherm constant in mmol $\cdot$ g$^{-1}$ $\cdot$ MPa$^{-1/n}$ and $n$ is the heterogeneity factor (dimensionless) that represents a deviation from the linearity of adsorption.

| | CVFF | COMPASS | COMPASS II | PCFF |
|---|---|---|---|---|
| $n$ | 8.2544 | 6.7383 | 6.2673 | 6.4320 |
| $k_F$ | 6.5762 | 5.4992 | 5.4290 | 4.6707 |
| $R^2$ | 0.9783 | 0.9961 | 0.9917 | 0.9882 |

### *3.2. Influence of temperature*

It was found using the MD method that in general the amount of methane molecules adsorbed by graphene decreases with increasing temperature (see Fig. 5). Gao *et al.* [39] stated that at high temperatures the pore structure of the graphene layers will alter and experience a blocking effect on the pore throat. Consequently, methane molecules cannot be adsorbed freely at a lower temperature. Moreover, when the temperature increases further the desorption process occurs. Fig. 5 illustrates that at 273 K the number density profile of methane is higher than at other temperature values, which agrees with other studies.

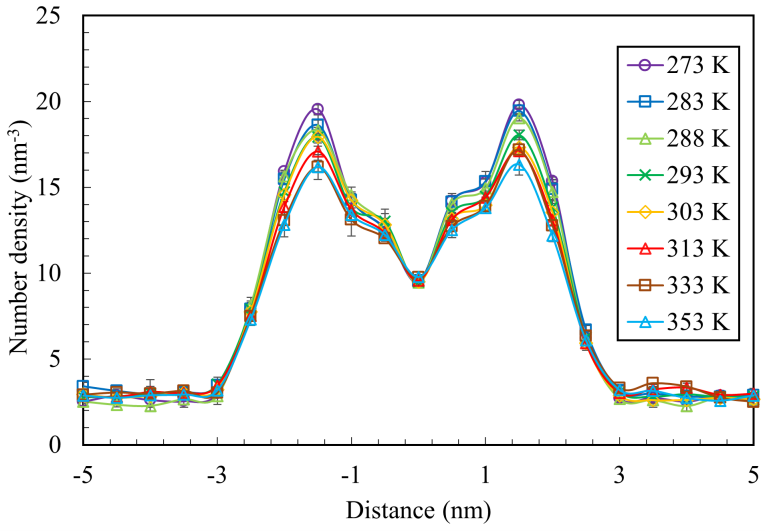


**Figure 5.** The influence of temperature on methane adsorption. Pore size of 1 nm. Error bars (± sample standard deviation (SD)) were included.

Similarly, the dependence of methane adsorption on temperature was analyzed using the GCMC method. It was found that with the increase in temperature, the loading amount of methane decreases as shown in Fig. 6. According to Xiong *et al.* [27] the mean kinetic energy of molecules increases as the temperature increases. This in turn increases the chances of molecules to overcome the van der Waals attraction forces exerted by the

Preprints (www.preprints.org) | NOT PEER-REVIEWED | Posted: 3 November 2022 doi:10.20944/preprints202211.0067.v1



graphene surface [26]. Thus, increasing the temperature results in a decrease of adsorption amount.

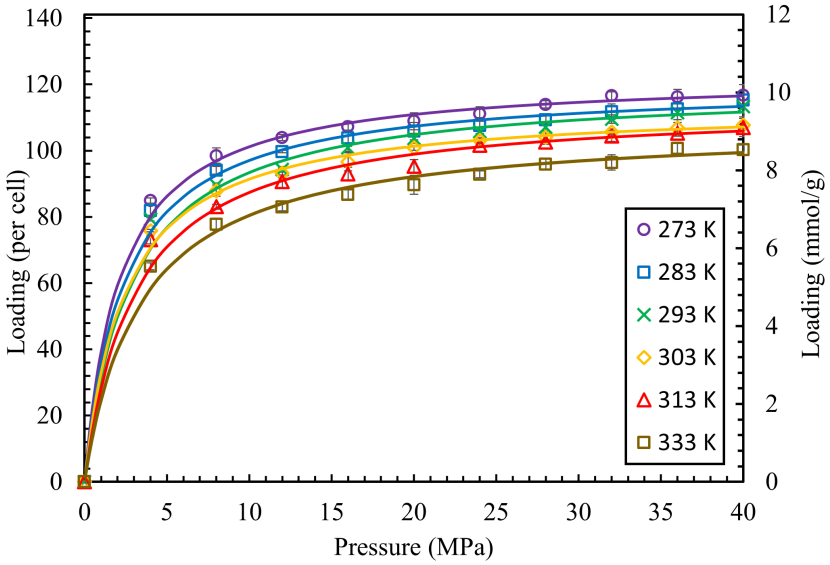


**Figure 6.** Adsorption isotherms of $CH_4$ molecule for the pore size of 1 nm and different temperatures. Error bars (± SD) were included and were smaller than the symbol size. The fitting parameters are given in Table 3

**Table 3.** Langmuir fitting parameters (see Eq. (1)) of the simulation results in Fig 6. $q_s$ is the maximum adsorption amount in mmol · g$^{-1}$, $K_L$ is the Langmuir adsorption constant in MPa$^{-1}$.

| | 273 K | 283 K | 293 K | 303 K | 313 K | 333 K |
|---|---|---|---|---|---|---|
| $q_s$ | 10.4392 | 10.2108 | 10.1591 | 9.6673 | 9.6934 | 9.1744 |
| $K_L$ | 0.4698 | 0.4215 | 0.3586 | 0.4102 | 0.3285 | 0.2926 |
| $R^2$ | 0.9995 | 0.9991 | 0.9988 | 0.9996 | 0.9985 | 0.9981 |

### *3.3. Influence of pore size*

As shown by the adsorption isotherms of methane, carbon dioxide and nitrogen gases in Fig. 7, adsorption isotherm increases with the pore size. This is due to the fact that as the pore size increases, more gas molecules can penetrate the slit pore, which leads to greater adsorption. The results of the simulations also show that the adsorption isotherms increase with pressure. This is because increasing the pressure results in more molecules striking the surface, favouring the adsorption process. Moreover, the loading of all three gases increases sharply at low pressures (0–4 MPa) and gradually slows down, which is in agreement with previous similar studies [25,40]. This can be explained by the fact that on the solid surface, there are a certain number of adsorption sites that can adsorb gas molecules. Thus, the number of adsorbed gas molecules increases linearly at the beginning. Once, all the available adsorption sites are filled, pressure no longer affects the adsorption rate. [40].

As can be seen from Fig. 8, the excess adsorption amounts of all three gases increase with the increase in pore size, for the same reason as the increase of total adsorption amounts. With regard to the pattern of the graph, the excess adsorption of all three gases increases until reaching a maximum, at around 5–8 MPa, and decreases afterwards, which is consistent with other studies [41,42]. This behaviour is explained by the fact that there are many available places for adsorption at lower pressures, meaning the density of the adsorbed state increases. Once all the available adsorption sites are filled, further increase in pressure does not affect the density of adsorbed state. The density of the bulk phase, on

Preprints (www.preprints.org) | NOT PEER-REVIEWED | Posted: 3 November 2022 doi:10.20944/preprints202211.0067.v1



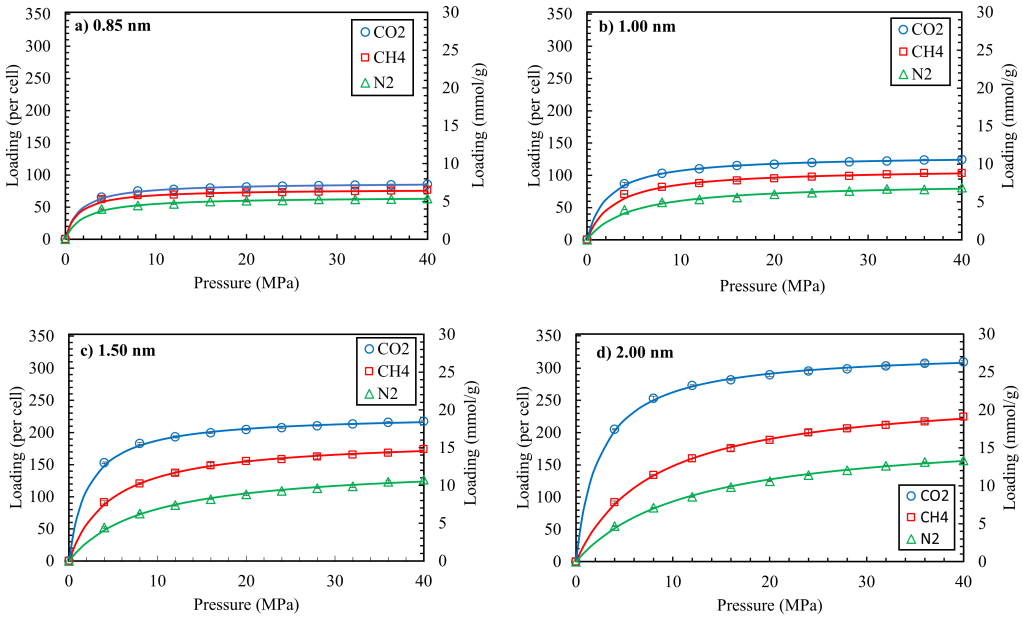


**Figure 7.** Adsorption isotherms of $CH_4$, $CO_2$ and $N_2$ molecules for the pore sizes of 0.85 nm (a), 1.00 nm (b), 1.50 nm (c) and 2.00 nm (d), and temperature of 318 K.

the other hand, always increases as pressure increases. Thus, the excess adsorption, which is the difference between the adsorbed state and bulk phase densities, increases at first and decreases to zero at higher pressures [24]. Moreover, there is maximum excess adsorption, which means there is an optimal pressure for maximum gas storage in slit pores [42].

According to Ottiger *et al.* [43], the methane and nitrogen excess adsorptions demonstrate a slight peak because the temperature in the shale exceeds their critical temperatures of −82.6 °Cand −147 °C [44], respectively. However, a distinctive trend can be observed for carbon dioxide, since its critical temperature, 31.2 °C [44], is close to the temperature in the shale. Its adsorption increases sharply at low pressures and decreases after reaching a maximum in the 5 to 8 MPa pressure range. An increase at the beginning is explained by a significant increase in the density of carbon dioxide when its phase changes from gaseous to supercritical state [45]. Similar to methane and nitrogen, the subsequent decrease in excess adsorption quantity is due to the filling up of the pores. The same tendency of carbon dioxide adsorption was observed in other studies [8,43,45–47].

The isosteric heat of all three gases was found to decrease with the increase in pore size, as shown in Fig. 9. This is because, at narrow pores (0.85 nm), only one layer of fluid is formed, which can directly interact with the graphene surface [31]. When the pore is wide enough for the formation of two (1.00 nm) or three (1.50 nm) fluid layers, the solid-fluid interaction becomes weaker, resulting in a decrease of the isosteric heat [31]. At higher pore sizes ($\geq$ 2.00 nm) more than three fluid layers are formed and the direct interaction of the fluid with the surface is not possible [31]. It can also be noted that the isosteric heats of all three gases increase with the increase in loading amount. According to several studies, the upward trend is attributed to an increase in the mutual attraction between adsorbate molecules with the increase of loading [31,35,38]. Moreover, the increasing behaviour of the isosteric heat with loading indicates the homogeneity of the graphene surface [35]. However, carbon dioxide experienced a sharper increase in isosteric heat than methane and nitrogen. This can be attributed to the fact that carbon dioxide molecules are more attracted to each other than to the carbon surface [48]. Finally, it was found that the isosteric heat of carbon dioxide is significantly higher than the isosteric heat of methane and nitrogen. This tendency signifies the stronger interaction of the adsorbent surface with $CO_2$ molecules rather than $CH_4$ or $N_2$ [40]. According to Abdulsalam *et al.* [32], the chemisorption process is indicated by the heat of adsorption being at least 80 kJ/mol. The isosteric heats of

Preprints (www.preprints.org) | NOT PEER-REVIEWED | Posted: 3 November 2022 doi:10.20944/preprints202211.0067.v1



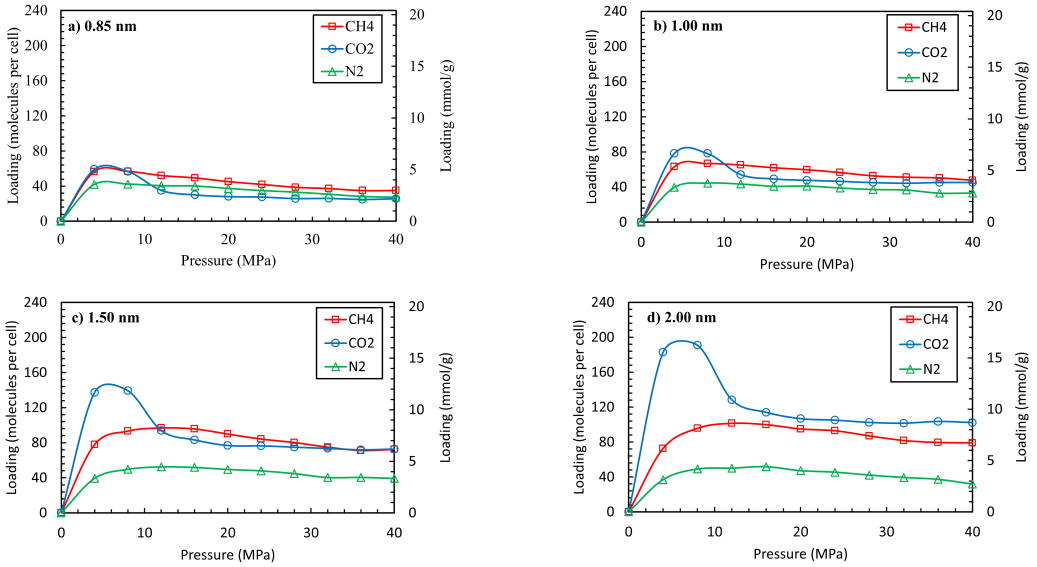


**Figure 8.** Excess adsorption isotherms of $CH_4$, $CO_2$ and $N_2$ molecules for the pore sizes of 0.85 nm (a), 1 nm (b), 1.5 nm (c) and 2 nm (d), and temperature of 318 K.

adsorption, in Fig. 9, obtained for different pore sizes are in the range of 12–24 kJ/mol for methane, 9–19 kJ/mol for nitrogen and 30–50 kJ/mol for carbon dioxide. These values are significantly less than that for chemisorption, meaning the adsorption of gas molecules on the graphene surface is physisorption. This finding is in agreement with other similar studies [32,38].

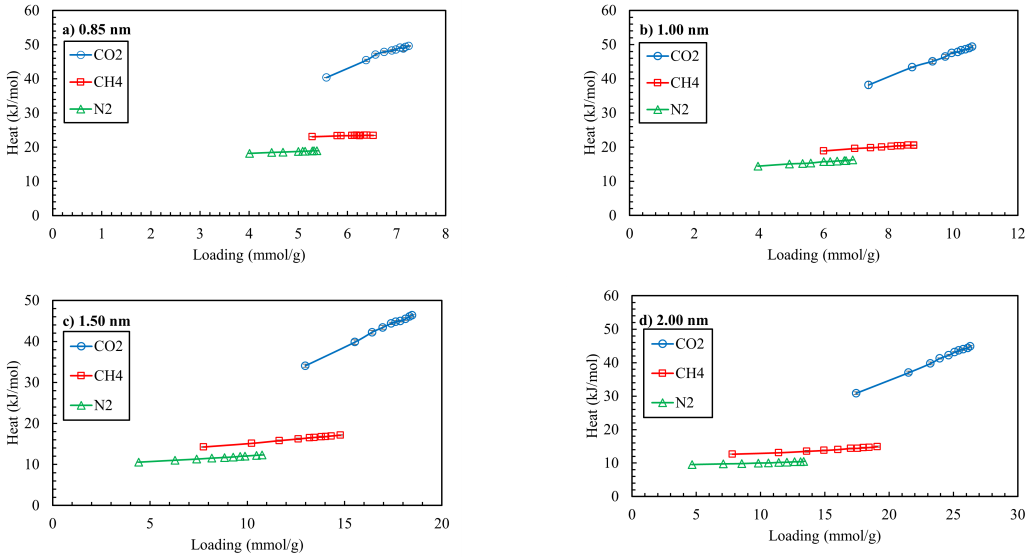


**Figure 9.** Isosteric heats of adsorption of $CH_4$, $CO_2$ and $N_2$ molecules for the pore sizes of 0.85 nm (a), 1.00 nm (b), 1.50 nm (c) and 2.00 nm (d), and temperature of 318 K.

To investigate the effect of the pore size on adsorption and study the adsorption structures, the number density distribution profiles of methane in different slit pores (0.6 nm, 0.7 nm, 1.0 nm, 1.5 nm and 2.0 nm) were shown in Fig. 10. The results are in good agreement with the simulation snapshots shown in Fig. 11. As is shown in Fig. 10, the minimum slit pore width at which methane molecules can penetrate the slit pore is 0.7 nm. With interlayer widths of 0.6 nm, the methane molecules cannot penetrate the slit pore (see Fig. 11a) since the radius of the methane, considering it as a spherical particle, is 0.38 nm [49] and adding 0.25 nm of the interlamellar distance between methane and

Preprints (www.preprints.org) | NOT PEER-REVIEWED | Posted: 3 November 2022 doi:10.20944/preprints202211.0067.v1



graphene molecules [50] gives 0.63 nm which is bigger than 0.6 nm. At an interlayer width of 0.7 nm, the methane molecules create a single adsorption layer in the centre of the pore (Fig. 11b). Two or more symmetrical peaks might occur due to the separation of the attractive potentials from the two walls by increasing pore size. At an interlayer width of 1 nm, the methane molecules create two adsorption layers with the lower peak of the number density distribution (Fig. 11c). For a slit pore size of 1.5 nm, the methane molecules create three adsorption layers (Fig. 11d). Note that the central peak has a much lower intensity than the main peaks at the edges. Finally, at an interlayer width of 2 nm, there are five adsorption layers (Fig. 11e). The central layer has the lowest intensity, and it could be neglected.

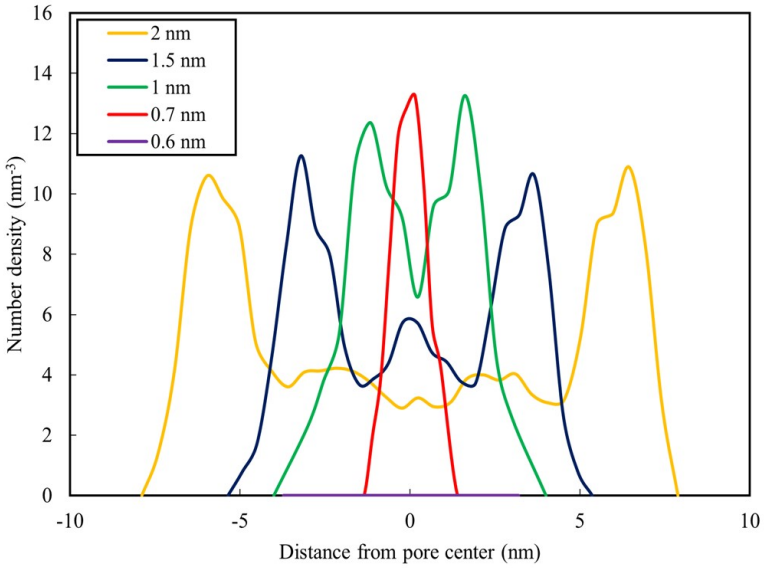


**Figure 10.** Number density profiles of $CH_4$ molecule at different slit pores (0.6 nm, 0.7 nm, 1.0 nm, 1.5 nm and 2.0 nm) based on the distance from the pore centre at temperature of 293 K

Preprints (www.preprints.org) | NOT PEER-REVIEWED | Posted: 3 November 2022 doi:10.20944/preprints202211.0067.v1



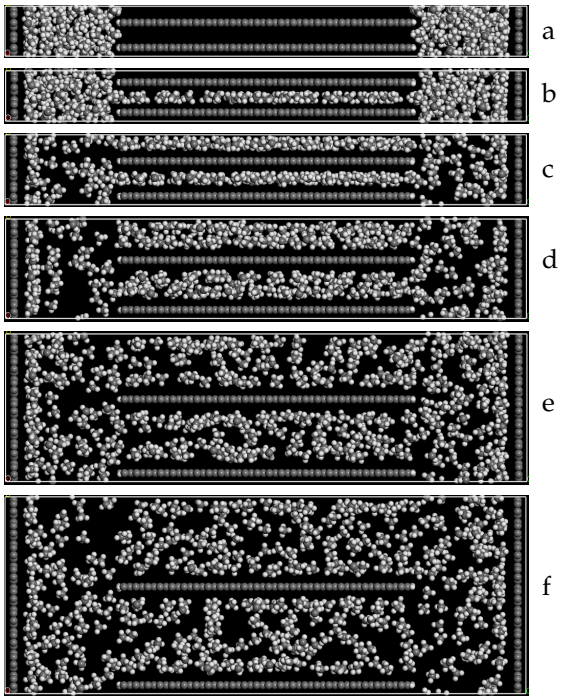


**Figure 11.** Snapshots for 3D models of methane adsorption in slit pores with different interlayer distances: a - 0.5 nm, b - 0.6 nm, c - 0.7 nm, d - 1 nm, e - 1.5 nm and f - 2 nm of slit pore size at 293 K

### *3.4. Displacement of adsorbed methane*

Displacement of loaded methane by $CO_2$ molecules starts from the adsorption of the $CO_2$ molecules on the vacancies. Since the adsorption capacity of $CO_2$ is stronger than the adsorption capacity of methane, $CO_2$ molecules might replace the adsorbed methane. Consequently, the adsorbed methane molecules dismiss from the graphene layers and return to the free phase. In Shi *et al.* [10], it was indicated that since the most probable interaction energy for methane is around -4.5 to -2.5 kJ $\cdot$ mol$^{-1}$ and for $CO_2$ is about -8.3 to -5.1 kJ $\cdot$ mol$^{-1}$, methane should be at the higher energy adsorption site, while $CO_2$ is at the lower energy adsorption site. In other words, the adsorption capacity of methane is weaker than the adsorption capacity of $CO_2$. In the case of $N_2$, the adsorption capacity of methane is stronger than the adsorption capacity of $N_2$, therefore the $N_2$ molecules can only adsorb on the vacancies and substitution does not occur. However, the $N_2$ molecules might cause desorption and displacement of the methane molecules since $N_2$ can isobarically decrease the partial pressure of methane [15]. Moreover, the displacement efficiency demonstrated a downward trend with the increase in temperature: with increasing temperature the number density profiles of $CO_2$ and $N_2$ started to behave similarly.

In experimental studies by Zhu *et al.* [51] and Turta *et al.* [52], it was found that $CO_2$ propagates through coal in a plug-like fashion, while $N_2$ moves more rapidly. The obtained results from Fig. 12 strongly correlate with those studies. In general, both gasses could displace the adsorbed methane efficiently. However, injecting $CO_2$ molecules resulted in a relatively slow breakthrough time and a sharp front. In contrast, a relatively fast breakthrough time and a wide front were observed while injecting $N_2$ molecules (Fig. 12). This can be explained by the fact that $CO_2$ travels slowly through the pore since it gets absorbed in the pore. In the case of $N_2$, it travels quickly through the pore since is less strongly adsorbed than $CH_4$. While $CO_2$ breaks through, the concentration of $CH_4$ decreases gradually. Similar results on the displacement process were also obtained by Wu *et al.* [15] using a coarse-grained united-atom model.

The radial distribution functions (RDFs) g(r) between $CH_4$, $CO_2$, $N_2$ and graphene (C) are shown in Fig. 13. For $CO_2$ and graphene layer, there is a distinct peak at $r \approx 1.2$ nm and relatively weaker peaks at $r \approx 4.5$ and 8.5 nm. The same tendency was observed for $CH_4$

Preprints (www.preprints.org) | NOT PEER-REVIEWED | Posted: 3 November 2022 doi:10.20944/preprints202211.0067.v1



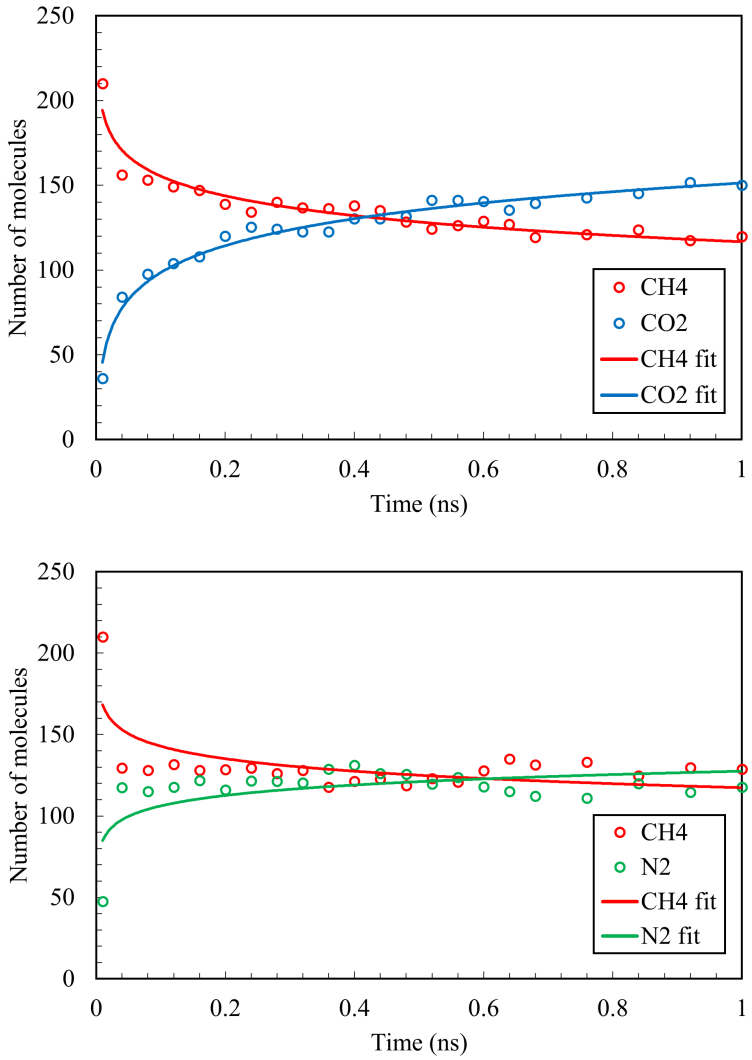


**Figure 12.** Evolution of the composition profiles of $CH_4$ displacement by a) $CO_2$ and $N_2$ at temperature of 293 K and pore size of 1.5 nm.

but with lower intensity. In the case of $N_2$, also the same peaks were determined, however, the intensity of the RDF curve of $N_2$ was lower than that of $CH_4$ which indicates that the arrangement of $CO_2$ molecules in the pores was more compact than those of $N_2$.

Fig. 14 presents the number density profiles of methane molecules at different temperatures. It was found that the injection of gases such as $CO_2$ and $N_2$ decreases the absorption of methane molecules, and at all temperature values, the number density of methane after gas injections was much lower than in the absence of the injection of gases. Recall that the adsorption capacity of the three gases decreases in the order of $CO_2$, $CH_4$ and $N_2$ (see Fig. 7). With a higher adsorption capacity, $CO_2$ molecules will displace methane molecules and be adsorbed more intensively than $N_2$ molecules. This is the primary reason why ESGR, which could be performed by displacement of $CH_4$ by $CO_2$, plays a vital role in the understanding of $CO_2$ sequestration. By comparing the adsorption isotherms of three gases in Fig. 7, it was found that for all the pore sizes, the value of nitrogen adsorption is the smallest and carbon dioxide adsorption is the greatest. This trend can be explained by the fact that the diameter of carbon dioxide molecules (0.33 nm [53]) is less than the diameter of methane (0.38 nm [53]) and nitrogen (0.36 nm [53]) molecules, meaning more carbon dioxide molecules can enter the pore rather than methane and nitrogen molecules.

Preprints (www.preprints.org) | NOT PEER-REVIEWED | Posted: 3 November 2022 doi:10.20944/preprints202211.0067.v1



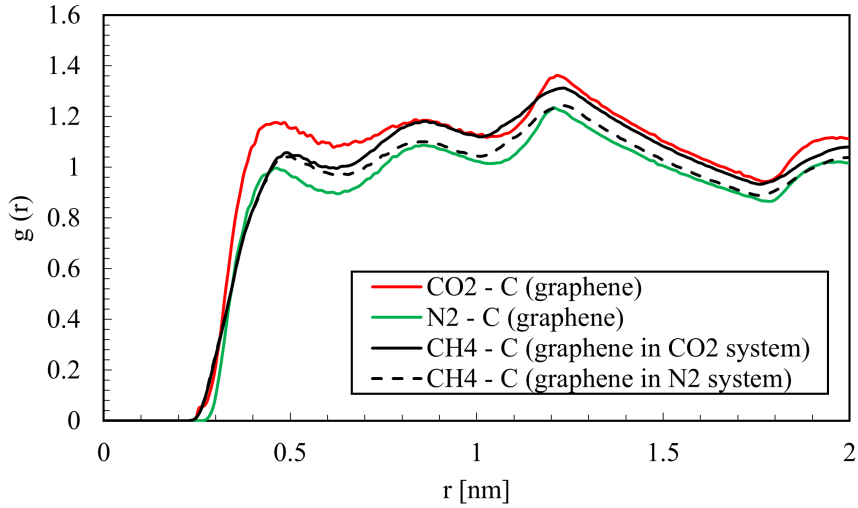


**Figure 13.** RDFs between carbon atoms of graphene and $CH_4$, $CO_2$ and $N_2$ gas molecules at 293 K and pore size of 1.5 nm.

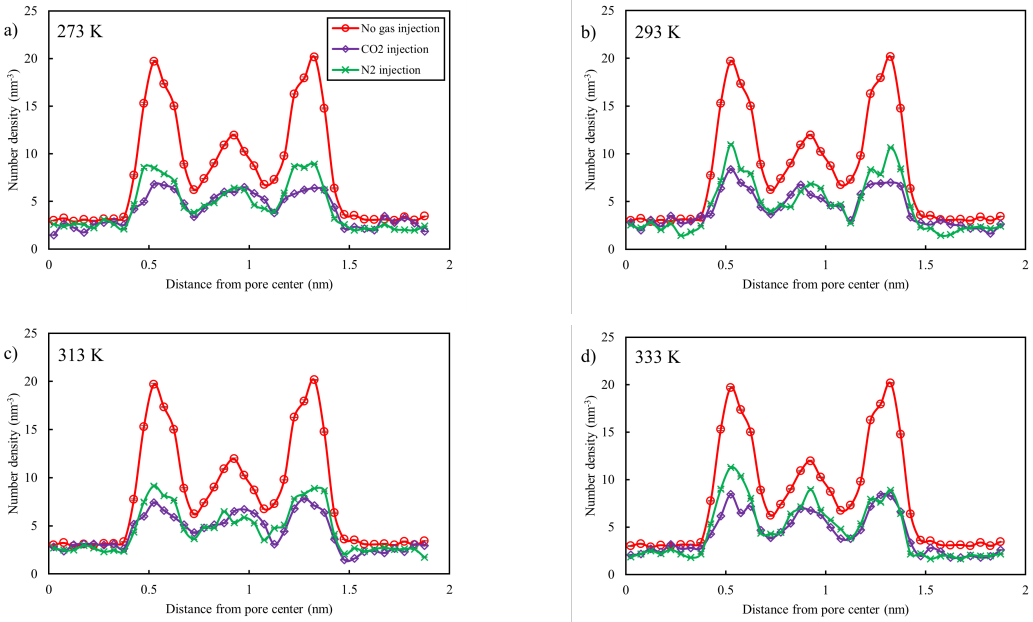


**Figure 14.** Number density profiles of $CH_4$ molecules for the pore size of 1.5 nm after injection of $CO_2$ and $N_2$ gasses under different temperature values: a) 273 K, b) 293 K, c) 313 K and d) 333 K. The figure legend shown in subfigure (a) applies to all subfigures.

## 4. Conclusions

In this study, the mechanisms of methane adsorption and displacement in slit pores are studied and identified using molecular dynamics modelling and grand canonical Monte Carlo simulations. The results show that CVFF forcefield gives the largest and PCFF gives the lowest adsorption amounts. COMPASS and COMPASS II demonstrate similar results. Because COMPASS and COMPASS II are relatively new methods and are found to be in better agreement with the experimental data, they were used for further simulations.

The minimum slit pore size at which molecules can penetrate the pore is 0.7 nm. As expected, with the increase of the slit pore's width, the adsorption amount increases and the adsorption structure of methane transitions from a single adsorption layer to multi

Preprints (www.preprints.org) | NOT PEER-REVIEWED | Posted: 3 November 2022 doi:10.20944/preprints202211.0067.v1



adsorption layers. In addition, the number of adsorbed molecules is found to increase with increasing pressure or decreasing temperature.

It was also found that the adsorption capacity of three gases decreases in the order $CO_2$, $CH_4$, $N_2$, meaning $CO_2$ can directly replace the methane molecules. Although the adsorption capacity of $N_2$ is lower, it can still replace methane by decreasing its partial pressure. Thus, it is concluded that both of the two gases can displace the adsorbed methane efficiently.

This study provides a detailed, microscopic-level understanding of the competitive adsorption mechanisms of methane, carbon dioxide, and nitrogen in organic nanopores common in shale gas and coalbed methane reservoirs. For future works, several topics need to be discussed and analyzed. For instance, in this work shale and coal rock minerals were simplified as graphene. However, it is also necessary to take into account the influence of other functional groups. Moreover, the effect of water and its competitive adsorption with methane on the organic pore surface needs to be investigated. In addition, it is highly necessary to explore the impact of gas flow at the nanoscale on methane adsorption and displacement in a broader sense.

**Author Contributions:** Investigation, formal analysis, data curation, visualization, Writing (original draft, review & editing): D.B. & S.A.; Conceptualization, Methodology, Review & editing, supervision, and funding acquisition: Y.W. & L.W.

**Funding:** This work was carried out with support from the "Simulation of sour gas injection EOR in tight carbonate reservoirs coupling capillarity and geomechanics" project (Grant Award Number 080420FD1918), the "Development of cryogenic fracturing technology for coalbed methane production in Karaganda Coal Basin, Kazakhstan" project (Grant Award Number 021220CRP2022), and the Social Policy Grant of Nazarbayev University. Lei Wang would like to thank the Science & Technology Department of Sichuan Province (2021YJ0355) for financial support.

**Informed Consent Statement:** Not applicable.

**Data Availability Statement:** Data will be available on request.

**Acknowledgments:** We acknowledge the National Supercomputing Center in Shenzhen for providing the computational resources and Materials Studio (version 7.0) software.

**Conflicts of Interest:** The authors declare no conflict of interest.

## Abbreviations

The following abbreviations are used in this manuscript:

| | |
|---|---|
| CBM | Coal Bed Methane |
| COMPASS | Condensed-phase Optimized Molecular Potentials for Atomistic Simulation Studies |
| COMPASS II | Condensed-phase Optimized Molecular Potentials for Atomistic Simulation Studies II |
| CVFF | Consistent Valence Forcefield |
| ESGR | Enhanced Shale Gas Recovery |
| GCMC | Grand Canonical Monte Carlo |
| GHG | Greenhouse gas |
| MD | Molecular Dynamics |
| PCFF | Polymer Consistent Forcefield |
| RDF | Radial Distribution Function |
| SD | Standard Deviation |
| SRK | Soave-Redlich-Kwong equation of state |

## References

1. U.S. Energy Information Administration - EIA - independent statistics and analysis.
2. Caulton, D.R.; Shepson, P.B.; Santoro, R.L.; Sparks, J.P.; Howarth, R.W.; Ingraffea, A.R.; Cambaliza, M.O.; Sweeney, C.; Karion, A.; Davis, K.J.; et al. Toward a better understanding and quantification of methane emissions from shale gas development. *Proceedings of the National Academy of Sciences* **2014**, *111*, 6237–6242. https://doi.org/10.1073/pnas.1316546111.
3. Qiao, L.; Wang, H.; Lu, S.; Liu, Y.; He, T. Novel Self-Adaptive Shale Gas Production Proxy Model and Its Practical Application. *ACS omega* **2022**, *7*, 8294–8305.

Preprints (www.preprints.org) | NOT PEER-REVIEWED | Posted: 3 November 2022 doi:10.20944/preprints202211.0067.v1




4. Huai, J.; Xie, Z.; Li, Z.; Lou, G.; Zhang, J.; Kou, J.; Zhao, H. Displacement behavior of methane in organic nanochannels in aqueous environment. *Capillarity* **2020**, *3*, 56–61.
5. Lyu, Q.; Tan, J.; Li, L.; Ju, Y.; Busch, A.; Wood, D.A.; Ranjith, P.G.; Middleton, R.; Shu, B.; Hu, C.; et al. The role of supercritical carbon dioxide for recovery of shale gas and sequestration in gas shale reservoirs. *Energy & Environmental Science* **2021**, *14*, 4203–4227.
6. Loucks, R.G.; Reed, R.M.; Ruppel, S.C.; Jarvie, D.M. Morphology, genesis, and distribution of nanometer-scale pores in siliceous mudstones of the Mississippian Barnett Shale. *Journal of sedimentary research* **2009**, *79*, 848–861. https://doi.org/10.2110/jsr.2009.092.
7. Sharma, A.; Namsani, S.; Singh, J.K. Molecular simulation of shale gas adsorption and diffusion in inorganic nanopores. *Molecular Simulation* **2015**, *41*, 414–422. https://doi.org/10.1080/08927022.2014.968850.
8. Liu, J.; Li, S.; Wang, Y. Molecular dynamics simulation of diffusion behavior of CH4, CO2, and N2 in mid-rank coal vitrinite. *Energies* **2019**, *12*, 3744.
9. Wang, L.; Cheng, Y.; Wang, Y. Laboratory study of the displacement coalbed CH4 process and efficiency of CO2 and N2 injection. *The Scientific World Journal* **2014**, *2014*, 242947. https://doi.org/10.1155/2014/242947.
10. Shi, J.; Gong, L.; Sun, S.; Huang, Z.; Ding, B.; Yao, J. Competitive adsorption phenomenon in shale gas displacement processes. *RSC Advances* **2019**, *9*, 25326–25335. https://doi.org/10.1039/C9RA04963K.
11. Hu, X.; Deng, H.; Lu, C.; Tian, Y.; Jin, Z. Characterization of CO2/CH4 competitive adsorption in various clay minerals in relation to shale gas recovery from molecular simulation. *Energy & Fuels* **2019**, *33*, 8202–8214.
12. Oudinot, A.Y.; Riestenberg, D.E.; Koperna, G.J. Enhanced Gas Recovery and CO2 Storage in Coal Bed Methane Reservoirs with N2 Co-Injection. *Energy Procedia* **2017**, *114*, 5356–5376. 13th International Conference on Greenhouse Gas Control Technologies, GHGT-13, 14-18 November 2016, Lausanne, Switzerland, https://doi.org/https://doi.org/10.1016/j.egypro.2017.03.1662.
13. Zheng, S.; Yao, Y.; Elsworth, D.; Liu, D.; Cai, Y. Dynamic Fluid Interactions during CO2-Enhanced Coalbed Methane and CO2 Sequestration in Coal Seams. Part 1: CO2–CH4 Interactions. *Energy & Fuels* **2020**, *34*, 8274–8282.
14. Becattini, V.; Gabrielli, P.; Antonini, C.; Campos, J.; Acquilino, A.; Sansavini, G.; Mazzotti, M. Carbon dioxide capture, transport and storage supply chains: Optimal economic and environmental performance of infrastructure rollout. *International Journal of Greenhouse Gas Control* **2022**, *117*, 103635. https://doi.org/https://doi.org/10.1016/j.ijggc.2022.103635.
15. Wu, H.; Chen, J.; Liu, H. Molecular dynamics simulations about adsorption and displacement of methane in carbon nanochannels. *The Journal of Physical Chemistry C* **2015**, *119*, 13652–13657. https://doi.org/10.1021/acs.jpcc.5b02436.
16. Lin, K.; Yuan, Q.; Zhao, Y.P. Using graphene to simplify the adsorption of methane on shale in MD simulations. *Computational Materials Science* **2017**, *133*, 99–107. https://doi.org/10.1016/j.commatsci.2017.03.010.
17. Zhao, J.; Wang, Z.; Guo, P. Microscopic simulation of methane adsorption in organic matter. *Industrial & Engineering Chemistry Research* **2019**, *58*, 3523–3530. https://doi.org/10.1021/acs.iecr.8b05762.
18. Taheri, Z.; Nakhaei Pour, A. Studying of the adsorption and diffusion behaviors of methane on graphene oxide by molecular dynamics simulation. *Journal of Molecular Modeling* **2021**, *27*, 1–8.
19. Xu, P.; Rahmani, F.; Chiew, Y.C. Adsorption and diffusion of methane and light gases in 3D nano-porous graphene sponge. *Molecular Simulation* **2022**, *48*, 882–890.
20. Baykasoglu, C.; Mert, H.; Deniz, C.U. Grand canonical Monte Carlo simulations of methane adsorption in fullerene pillared graphene nanocomposites. *Journal of Molecular Graphics and Modelling* **2021**, *106*, 107909.
21. Cheng, X.; Li, Z.; He, Y.L. Release of methane from nanochannels through displacement using CO 2. *RSC advances* **2021**, *11*, 15457–15466.
22. Frenkel, D.; Smit, B. *Understanding molecular simulation: from algorithms to applications*; Vol. 1, Elsevier, 2001.
23. Foo, K.Y.; Hameed, B.H. Insights into the modeling of adsorption isotherm systems. *Chemical engineering journal* **2010**, *156*, 2–10.
24. Mosher, K.; He, J.; Liu, Y.; Rupp, E.; Wilcox, J. Molecular simulation of methane adsorption in micro-and mesoporous carbons with applications to coal and gas shale systems. *International Journal of Coal Geology* **2013**, *109*, 36–44.
25. Zhou, S.; Wang, H.; Li, B.; Li, S.; Sepehrnoori, K.; Cai, J. Predicting adsorbed gas capacity of deep shales under high temperature and pressure: Experiments and modeling. *Advances in Geo-Energy Research* **2022**, *6*, 482–491.
26. Ammendola, P.; Raganati, F.; Chirone, R. CO2 adsorption on a fine activated carbon in a sound assisted fluidized bed: Thermodynamics and kinetics. *Chemical Engineering Journal* **2017**, *322*, 302–313.
27. Xiong, J.; Liu, X.J.; Liang, L.X.; Zeng, Q. Investigation of methane adsorption on chlorite by grand canonical Monte Carlo simulations. *Petroleum Science* **2017**, *14*, 37–49.
28. Talu, O.; Myers, A.L. Molecular simulation of adsorption: Gibbs dividing surface and comparison with experiment. *AIChE journal* **2001**, *47*, 1160–1168.
29. Busch, A.; Gensterblum, Y. CBM and CO2-ECBM related sorption processes in coal: a review. *International Journal of Coal Geology* **2011**, *87*, 49–71.
30. Soave, G. Equilibrium constants from a modified Redlich-Kwong equation of state. *Chemical engineering science* **1972**, *27*, 1197–1203.
31. Hlushak, S. Heat of adsorption, adsorption stress, and optimal storage of methane in slit and cylindrical carbon pores predicted by classical density functional theory. *Physical Chemistry Chemical Physics* **2018**, *20*, 872–888.
32. Abdulsalam, J.; Mulopo, J.; Bada, S.O.; Oboirien, B. Equilibria and Isosteric Heat of Adsorption of Methane on Activated Carbons Derived from South African Coal Discards. *ACS omega* **2020**, *5*, 32530–32539.

Preprints (www.preprints.org) | NOT PEER-REVIEWED | Posted: 3 November 2022 doi:10.20944/preprints202211.0067.v1




33. Sims, R.A.; Harmer, S.L.; Quinton, J.S. The role of physisorption and chemisorption in the oscillatory adsorption of organosilanes on aluminium oxide. *Polymers* **2019**, *11*, 410.
34. Hsu, S.C.; Lu, C.; Su, F.; Zeng, W.; Chen, W. Thermodynamics and regeneration studies of CO2 adsorption on multiwalled carbon nanotubes. *Chemical Engineering Science* **2010**, *65*, 1354–1361.
35. Yuan, B.; Wu, X.; Chen, Y.; Huang, J.; Luo, H.; Deng, S. Adsorption of CO2, CH4, and N2 on ordered mesoporous carbon: approach for greenhouse gases capture and biogas upgrading. *Environmental science & technology* **2013**, *47*, 5474–5480.
36. Khalkhali, M.; Ghorbani, A.; Bayati, B. Study of adsorption and diffusion of methyl mercaptan and methane on FAU zeolite using molecular simulation. *Polyhedron* **2019**, *171*, 403–410. https://doi.org/10.1016/j.poly.2019.07.038.
37. Rexer, T.F.; Benham, M.J.; Aplin, A.C.; Thomas, K.M. Methane adsorption on shale under simulated geological temperature and pressure conditions. *Energy & Fuels* **2013**, *27*, 3099–3109.
38. Zhou, S.; Wang, H.; Zhang, P.; Guo, W. Investigation of the isosteric heat of adsorption for supercritical methane on shale under high pressure. *Adsorption Science & Technology* **2019**, *37*, 590–606.
39. Gao, Z.; Ma, D.; Chen, Y.; Zheng, C.; Teng, J. Study for the effect of temperature on methane desorption based on thermodynamics and kinetics. *ACS omega* **2020**, *6*, 702–714. https://doi.org/10.1021/acsomega.0c05236.
40. You, J.; Tian, L.; Zhang, C.; Yao, H.; Dou, W.; Fan, B.; Hu, S. Adsorption behavior of carbon dioxide and methane in bituminous coal: A molecular simulation study. *Chinese Journal of Chemical Engineering* **2016**, *24*, 1275–1282.
41. Zhang, J.; Liu, K.; Clennell, M.; Dewhurst, D.; Pan, Z.; Pervukhina, M.; Han, T. Molecular simulation studies of hydrocarbon and carbon dioxide adsorption on coal. *Petroleum Science* **2015**, *12*, 692–704.
42. Sui, H.; Yao, J.; Zhang, L. Molecular simulation of shale gas adsorption and diffusion in clay nanopores. *Computation* **2015**, *3*, 687–700.
43. Ottiger, S.; Pini, R.; Storti, G.; Mazzotti, M.; Bencini, R.; Quattrocchi, F.; Sardu, G.; Deriu, G. Adsorption of pure carbon dioxide and methane on dry coal from the Sulcis Coal Province (SW Sardinia, Italy). *Environmental Progress* **2006**, *25*, 355–364.
44. Perry, R.H.; Green, D.W.; Perry, R.H. *Perry's Chemical Engineers' handbook*; McGraw-Hill, 2008.
45. Weniger, P.; Kalkreuth, W.; Busch, A.; Krooss, B.M. High-pressure methane and carbon dioxide sorption on coal and shale samples from the Paraná Basin, Brazil. *International Journal of Coal Geology* **2010**, *84*, 190–205.
46. Busch, A.; Alles, S.; Gensterblum, Y.; Prinz, D.; Dewhurst, D.N.; Raven, M.D.; Stanjek, H.; Krooss, B.M. Carbon dioxide storage potential of shales. *International journal of greenhouse gas control* **2008**, *2*, 297–308.
47. Merey, S.; Sinayuc, C. Analysis of carbon dioxide sequestration in shale gas reservoirs by using experimental adsorption data and adsorption models. *Journal of Natural Gas Science and Engineering* **2016**, *36*, 1087–1105.
48. Krungleviciute, V.; Migone, A.D.; Yudasaka, M.; Iijima, S. CO2 adsorption on dahlia-like carbon nanohorns: isosteric heat and surface area measurements. *The Journal of Physical Chemistry C* **2012**, *116*, 306–310.
49. Mohamad, M.B.; Fong, Y.Y.; Shariff, A. Gas separation of carbon dioxide from methane using polysulfone membrane incorporated with Zeolite-T. *Procedia engineering* **2016**, *148*, 621–629. https://doi.org/10.1016/j.proeng.2016.06.526.
50. Yang, N.; Yang, D.; Zhang, G.; Chen, L.; Liu, D.; Cai, M.; Fan, X. The effects of graphene stacking on the performance of methane sensor: a first-principles study on the adsorption, band gap and doping of graphene. *Sensors* **2018**, *18*, 422. https://doi.org/10.3390/s18020422.
51. Zhu, J.; Jessen, K.; Kovscek, A.R.; Orr, F.M. Analytical theory of coalbed methane recovery by gas injection. *SPE journal* **2003**, *8*, 371–379.
52. Turta, A.T.; Sim, S.S.; Singhal, A.K.; Hawkins, B.F. Basic investigations on enhanced gas recovery by gas-gas displacement. *Journal of Canadian Petroleum Technology* **2008**, *47*.
53. Shieh, J.J.; Chung, T.S. Gas permeability, diffusivity, and solubility of poly (4-vinylpyridine) film. *Journal of Polymer Science Part B: Polymer Physics* **1999**, *37*, 2851–2861.